Implementation of Microchannel Evaporator for High-Heat-Flux Refrigeration Cooling Applications

Jaeseon Lee

Issam Mudawar[1]
e-mail: mudawar@ecn.purdue.edu

Purdue University International
Electronic Cooling Alliance,
West Lafayette, IN 47907

While most recently electronic cooling studies have been focused on removing the heat from high-power-density devices, the present study also explores means of greatly decreasing the device operating temperature. This is achieved by incorporating a microchannel heat sink as an evaporator in an R134a refrigeration loop. This system is capable of maintaining device temperatures below 55°C while dissipating in excess of 100 W/cm^2. It is shown that while higher heat transfer coefficients are possible with greater mass velocities, those conditions are typically associated with wet compression corresponding to evaporator exit quality below unity and liquid entrainment at the compressor inlet. Wet compression compromises compressor performance and reliability as well as refrigeration cycle efficiency and therefore must be minimized by maintaining only slightly superheated conditions at the compressor inlet, or using a wet-compression-tolerant compressor. A parametric study of the effects of channel geometry on heat sink performance points to channels with small width and high aspect ratio as yielding superior thermal performance corresponding to only a modest penalty in pressure drop.
[DOI: 10.1115/1.2159006]

1 Introduction

While thermal management of high-heat-flux electronic devices has attracted significant attention in recent years, much of the published work concerns mainly the heat removal requirements. The heat is typically removed by a liquid coolant and ultimately rejected to ambient air. As heat flux levels continue to escalate, there is increasing concern over the ability to maintain acceptable device temperatures for an essentially fixed ambient air temperature. This is because of the appreciable thermal resistance comprised of not only the coolant's convection resistance, but the conduction resistance across the device itself and any intermediate bond/solder layers. This points to refrigeration cooling as an effective means for greatly reducing the coolant's temperature and therefore maintaining acceptable device temperatures when dissipating very high heat fluxes. The present study concerns the development of a liquid cooling scheme that capitalizes upon the merits of both high-performance micro-channel flow boiling and refrigeration cooling.

Many researchers have explored the merits of microchannel heat sinks and demonstrated a notable enhancement in cooling performance compared to other liquid cooling schemes. This was quite evident from an early study by Tuckerman and Pease [1] who used a single-phase liquid-cooled heat sink. But while their heat sink was quite effective at dissipating the heat, its reliance on sensible heating the coolant resulted in detrimental streamwise temperature gradients along both coolant and heat sink. Reducing these gradients by increasing the coolant's flow rate was complicated by the appreciable pressure drop associated with microchannel flow. Bowers and Mudawar [2] showed how better temperature uniformity can be realized using two-phase microchannel heat sinks, which remove the heat more isothermally by latent instead of sensible heat.

With its abundance, low cost and superior thermophysial properties, water has been the coolant of choice for many single-phase and two-phase micro-channel heat sink applications [3,4]. Its drawbacks, however, are (1) poor dielectric properties, which can produce arcing/shorting in electronic devices, and (2) high saturation temperature. At one atmosphere, the saturation temperature of water (100°C) precludes maintaining acceptable device temperatures. Lower saturation temperatures are possible at subatmospheric pressure, but the low pressures necessary at maintaining acceptable temperatures are known to initiate undesirable bubble nucleation effects [5], let alone the increased likelihood of air inclusion due to any system leaks.

Dielectric fluorochemical coolants such as FC-72, FC-87, and PF-5052 circumvent the aforementioned arcing/shorting problem. They also possess lower saturation temperatures at one atmosphere. Unfortunately their thermophysical properties are far inferior to those of water, and achieving acceptable device temperatures requires implementing effective surface augmentation techniques and/or supplying the coolant at a relatively high mass velocity [6].

Refrigeration cooling resolves the high device temperature concerns as well as provides the added benefits of faster switching time (due to increased electron mobility) and therefore better device performance, as well as reduced current leakage [7]. Those combined advantages lead to the introduction of several commercial refrigeration cooled computer systems in the last decade [7].

With a refrigeration system, the coolant's saturation temperature is greatly decreased, sometimes far below subfreezing temperatures. However, refrigeration requires increasing operation pressure, which contributes both added cost and complexity to a cooling system.

This paper addresses the challenge of incorporating a two-phase microchannel heat sink as an evaporator in a vapor compression refrigeration system. Recent studies by the authors have yielded new correlations for pressure drop and two-phase heat transfer coefficient for refrigerant-cooled microchannel heat sinks [8,9]. This study will utilize these correlations to explore several fundamental thermal aspects of the heat sink that were passed over in a

[1]Author to whom correspondence should be addressed.

Contributed by the Electronic and Photonic Packaging Division of ASME for publication in the JOURNAL OF ELECTRONIC PACKAGING. Manuscript received September 7, 2004; final manuscript received June 17, 2005. Review conducted by Bahgat Sammakia.

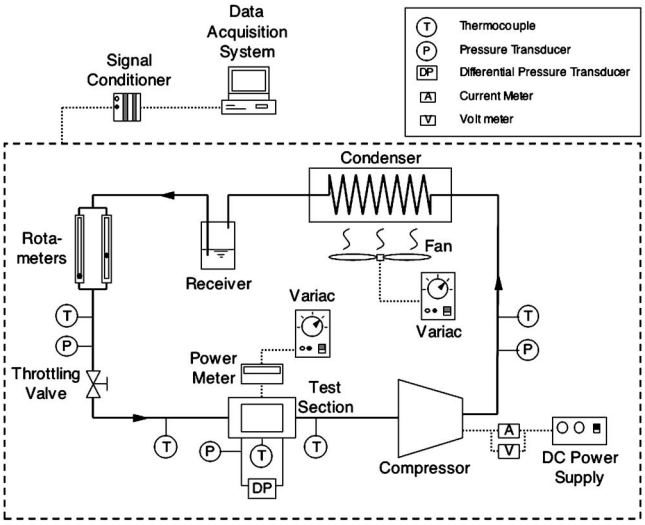

Fig. 1 Schematic of test loop

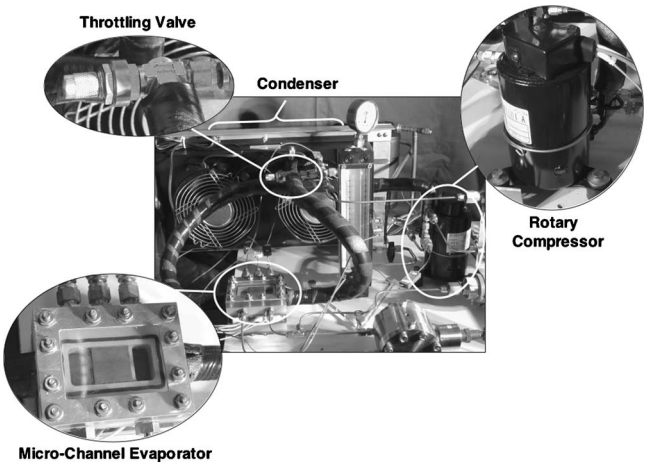

Fig. 3 Pictures of facility and key components

past commercial trial. Examined here is the effectiveness of the heat sink at removing high heat fluxes while maintaining low device temperatures, as well as the complex relationship between device heat flux, device temperature, and coolant operating conditions in the evaporator, and means of optimizing operating conditions in pursuit of better overall cooling performance and sound refrigeration system operation.

2 Experimental Methods

2.1 Apparatus and Measurement Techniques. Figure 1 shows a schematic diagram of the vapor compression refrigeration flow loop constructed for this study. The microchannel test module is incorporated as the evaporator for the refrigeration loop. The working fluid used is R134a, a HFC refrigerant popular throughout the refrigeration industry for its nonozone-depleting attributes.

Figure 2 shows the microchannel heat sink that consists of a transparent polycarbonate (Lexan) cover plate, a G-10 fiberglass housing, a microchannel oxygen-free copper heat sink, and a G-10 support plate. Heat is provided by three cartridge heaters that are embedded in the copper heat sink, simulating heat dissipation from an electronic device. The microchannels are formed by cutting 53 of 231 μm wide and 713 μm deep microslots into the 25.3 mm $\times$ 25.3 mm top surface of the copper heat sink. The top walls of the microchannels are formed by clamping the cover plate atop the heat sink. The G-10 housing includes upstream and downstream plenums to both ensure uniform flow distribution between the microchannels and provide convenient locations for pressure and temperature sensors. Following assembly, insulating glass fiber is wrapped around the outside of the heat sink to guard against heat loss. Electric power to the cartridge heaters is provided by a variac and measured by a power meter.

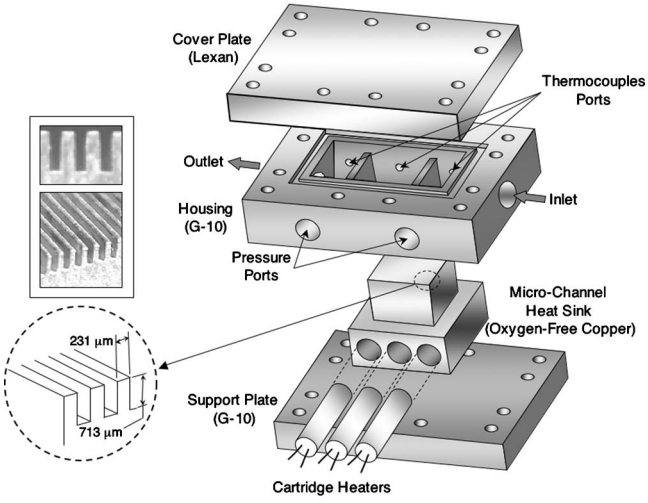

Fig. 2 Structure of microchannel evaporator test section

A rotary compressor is used whose power is supplied from a dc power source. The condenser has a conventional fin-tube construction and is fitted with an axial fan. Air cooling is achieved by adjusting fan speed with the aid of a variac, providing the required condenser exit subcooling. The throttling device consists of a manual metering valve, which is situated upstream of the microchannel evaporator test section. Figure 3 depicts photos of key components of the test facility.

Each of the refrigeration cycle node states is measured with a type-T thermocouple and a pressure transducer as indicated in Fig. 1. Another type-K thermocouple is inserted halfway along the heat sink block, Fig. 4, to measure the heat sink wall temperature at the same axial location. An absolute pressure transducer and a differential pressure transducer are used to measure inlet plenum pressure and pressure drop between the two plenums, respectively. All sensor outputs are transferred to a signal conditioner interfaced to a data acquisition PC. The system flow rate is measured downstream from the condenser by a rotameter, which also makes it possible to visually ensure subcooled liquid state at the same location.

The rotameter provided better than 2% accuracy in flow rate measurement. Errors in the pressure transducer and thermocouple measurements were less than 0.5% and $\pm 0.3^{\circ}$C, respectively. Heat loss from the heat sink was estimated at less than 4% of the electrical power input.

2.2 Operating Conditions. The refrigerant exits the rotary compressor in a superheated vapor state and is returned to liquid after passing through the condenser. This subcooled liquid is throttled into a two-phase mixture by flashing through the metering valve. This provides a two-phase mixture at the evaporator inlet as in most refrigeration systems. Vapor quality increases as the refrigerant is heated inside the evaporator.

The mass flow rate was determined by multiplying the volumetric flow rate of liquid upstream of the throttling valve and the density of liquid at the condenser outlet, obtained from temperature and pressure measurement at the same location. Since the throttling process is isenthalpic, the evaporator inlet enthalpy was

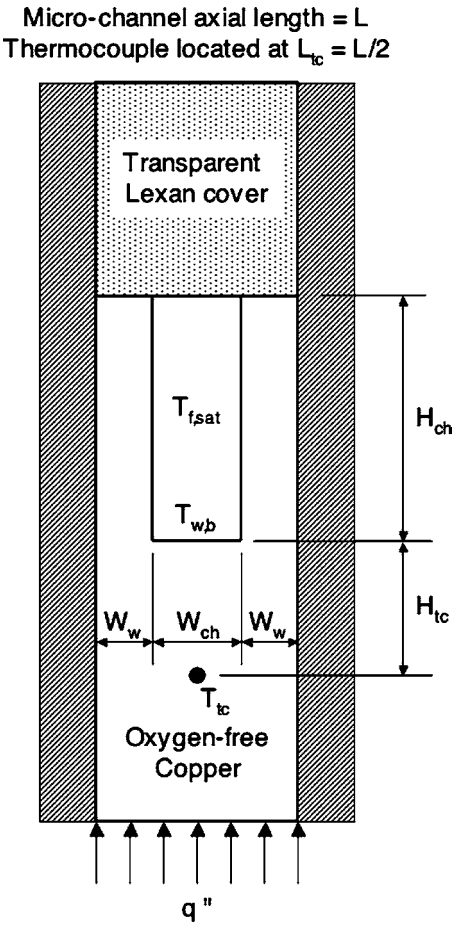

Fig. 4 Channel unit cell geometry

determined from the enthalpy of liquid based on liquid temperature and pressure measured upstream of the throttling valve. The evaporator's inlet quality, $x_{e,\text{in}}$, was determined from this enthalpy value and the evaporator's inlet temperature or pressure measurements. Experimental data were acquired over the following range of evaporator parameters: inlet pressure of $P_{\text{in}}=1.44-6.60$ bar, inlet quality of $x_{e,\text{in}}=0.001-0.25$, outlet quality of $x_{e,\text{out}}=0.49$–superheat, mass velocity of $G=127-654$ kg/m^2 s, and heat input of $Q_{\text{evap}}=100-600$ W.

3 Experimental Results

A key parameter for assessment of the microchannel heat sink's cooling performance is the measured heat sink temperature, T_{tc}. As illustrated in Fig. 4, this temperature was measured by a type-K thermocouple situated a short distance beneath the base of the microchannels halfway along the heat sink. The fluid at the same axial location is in saturated state for all operating conditions. Figure 5 shows variations of the heat sink temperature and saturation temperature with mass velocity for four different values of evaporator heat load. The saturation temperature was determined from the measured evaporator inlet conditions using a two-phase pressure drop correlation recently developed by the authors for R134a [8]. For a fixed evaporator thermal load, the mass velocity was modulated by the throttling valve. Increased throttling at low mass velocities produced appreciable pressure drop across the throttling valve. Both the copper and refrigerant temperatures show mild decreases with decreasing mass velocity, which is followed by a big departure between the two temperatures at low mass velocities. When the compressor was operated within its normal capacity range, the copper block temperature curves indicate a minimum optimized cooling point. However, this optimal point is not evident outside the normal range (e.g., for $Q_{\text{evap}}=500$ W).

This trend is closely associated with the transition from wet to dry compression. Figure 6 shows a *P-h* diagram of the present refrigeration cycle for an evaporator thermal load of 200 W and two mass velocities. At the higher mass velocity of $G=343$ kg/m^2 s, the refrigerant exits the evaporator as a two-phase mixture corresponding to wet compression (i.e., with liquid present at the compressor inlet). This condition is undesirable for most compressors. For example, reciprocating compressors are designed to shut down under such wet inlet conditions. On the other hand, rotary compressors can tolerate some wet compression, though their performance may be greatly degraded, let alone the potential damage to their mechanical components. Figure 6 shows the lower mass velocity of $G=128$ kg/m^2 s producing superheated evaporator outlet conditions and dry compression. The compressor performance in this case is greatly enhanced, producing a far greater compression ratio than that with wet compression. For a fixed condenser side temperature, dry compression also causes appreciable reduction in the evaporator side refrigerant temperature compared to wet compression.

Returning to Fig. 5, the copper to fluid temperature difference (measure of thermal resistance of microchannel heat sink) is fairly constant (less than 0.1°C/W under most evaporator thermal load conditions) for wet compression conditions associated with high mass velocities. However, once dry compression commences as mass velocity is decreased, the thermal resistance begins to increase sharply.

Figure 7 shows the variation of the refrigeration cycle's coefficient of performance (COP) with mass velocity for three evaporator thermal loads. These three cases are within the normal capacity range of the compressor. A far greater COP value is achieved for thermal loads that are higher than the normal range (e.g., $Q_{\text{evap}}=500$ W). COP is defined here as the ratio of evaporator thermal load to compressor power consumption. COP is highly degraded for wet compression conditions associated with high mass velocities, and greatly enhanced with dry compression at low mass velocities. Notice, however, that further reduction in mass velocity causes a slight decline in COP, especially notable for $Q_{\text{evap}}=100$ W. This can be explained by the greater superheat at the compressor inlet producing a larger specific volume of vapor, which requires greater compressor power for the same compression rate, i.e., yields a lower COP.

One may speculate a similar reduction in COP due to the increased specific volume caused by the relatively large pressure drop of a two-phase microchannel evaporator. While the pressure drop per unit length is much greater for a microchannel than for a conventional evaporator, it should be emphasized that the evaporator in this study is intended as a heat sink for a relatively short electronic device, so the evaporator pressure drop is fairly small even if the pressure gradient is large. This implies the effect of evaporator pressure drop on cycle performance is negligible. The *P-h* diagram in Fig. 6 clearly demonstrates this point.

Overall, the compressor suction (inlet) condition poses a fundamental challenge to implementing microchannel refrigeration cooling in electronic applications. On one hand, higher heat removal rates are possible with a lower evaporator exit quality, i.e., wet compression. On the other hand, optimum cycle performance and compressor reliability favor dry compression. Furthermore, heat dissipation from an electronic device is not constant during normal device operation. This points to the need to incorporate an adaptive control system (e.g., using a thermostatic expansion valve) to maintain minimal superheat at the compressor inlet.

4 Heat Sink Temperature Distribution

Aside from the need to remove the heat dissipated from an electronic device, the device temperature must be maintained as low and uniform as possible in order to minimize thermal stresses

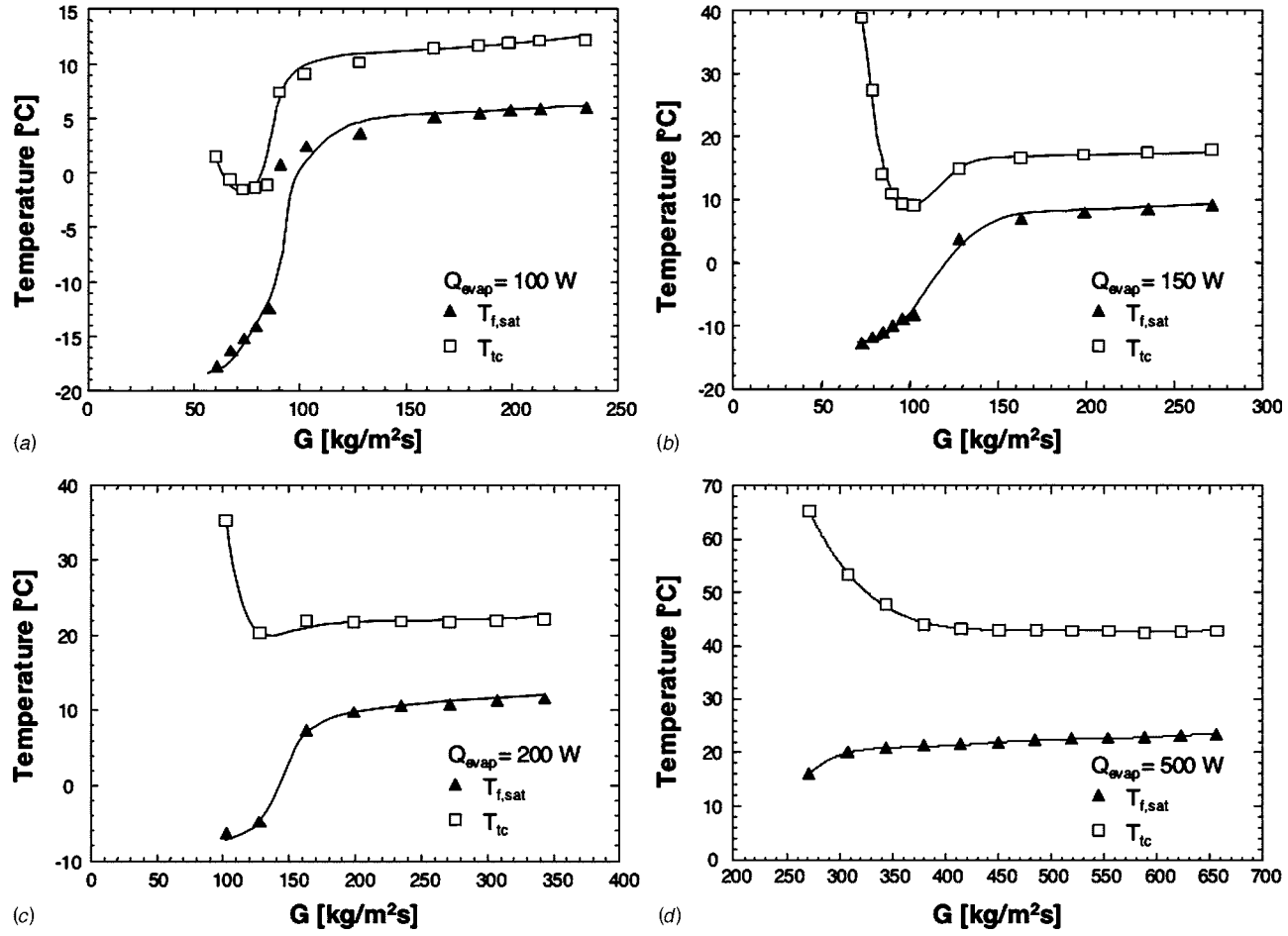

Fig. 5 Variation of measured copper temperature with mass velocity for evaporator heat loads of (*a*) 100, (*b*) 150, (*c*) 200, and (*d*) 500 W

that can trigger mechanical failure. Since it is quite difficult to measure the temperature distribution along the heat sink, this distribution was inferred using correlations for two-phase pressure drop and heat transfer coefficient that were recently developed by the authors for R134a-cooled microchannel heat sink evaporators [8,9] and are summarized in Table 1. The thermodynamic equilibrium quality at any distance z along a microchannel was calculated from the simple heat balance

$$x_{e,z} - x_{e,\text{in}} = \frac{4q''z}{Gd_h h_{fg}}. \tag{1}$$

The local refrigerant saturation temperature was obtained from the saturated pressure determined from the pressure drop model.

Figure 8 shows the calculated variations of quality, x_e, two-phase heat transfer coefficient, h_{tp}, and heat-sink base-wall tem-

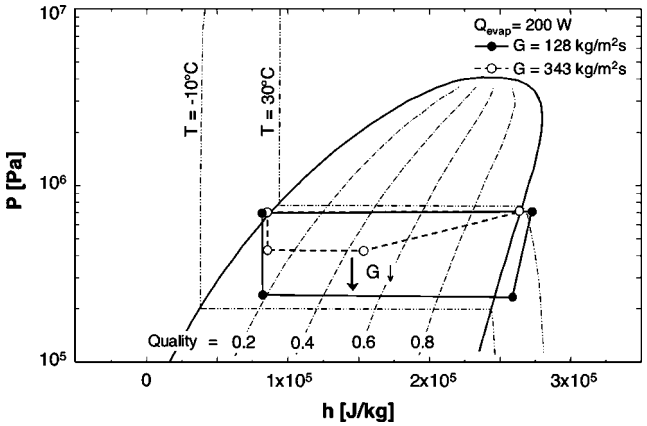

Fig. 6 Pressure-enthalpy (*P-h*) diagram for two evaporator mass velocities

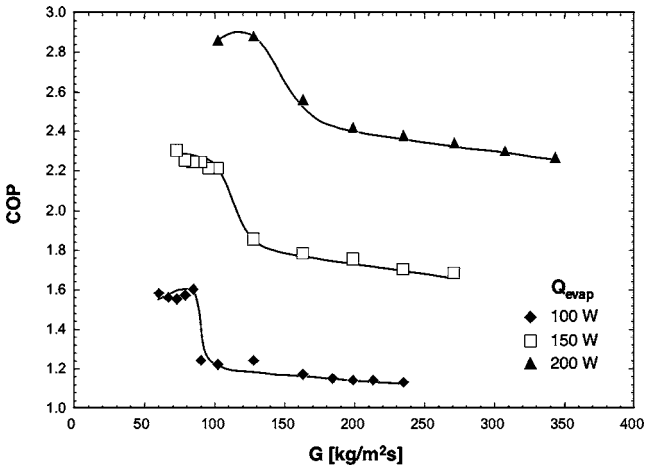

Fig. 7 Variation of cycle COP with mass velocity for three evaporator heat loads

Table 1 Correlations for pressure drop and local boiling heat transfer coefficient

	Correlations
Two-phase pressure drop [8]	$\Delta P_{\text{tot}} = \Delta P_c + (\Delta P_f + \Delta P_a)_{\text{tp}} + \Delta P_{\text{sp},g} - \Delta P_e$
	$\Delta P_c = \frac{G^2 v_f}{2}\left[\left(\frac{1}{C_c} - 1\right)^2 + \left(1 - \frac{1}{\sigma_c^2}\right)\right]\left[1 + \frac{v_{fg} x_{e,\text{in}}}{v_f}\right]$
	$\Delta P_e = G^2 \sigma_e (1 - \sigma_e) v_f \left[1 + \frac{v_{fg} x_{e,\text{out}}}{v_f}\right]$
	$\Delta P_f = \frac{2G^2 L_{\text{tp}}}{d_h x_{e,\text{out}}} \int_{x_{e,\text{in}}}^{x_{e,\text{out}}} f_f (1 - x_e) v_f \phi_f^2 dx_e$
	$\phi_f^2 = 1 + \frac{C}{X} + \frac{1}{X^2}, X^2 = \frac{(dp/dz)_f}{(dp/dz)_g}$
	$C_{vv} = 2.16\,\text{Re}_{fo}^{0.047}\,\text{We}_{fo}^{0.60}$ (laminar liquid-laminar vapor) $C_{vt} = 1.45\,\text{Re}_{fo}^{0.25}\,\text{We}_{fo}^{0.23}$ (laminar liquid-turbulent vapor)
	$\Delta P_a = G^2\left\{\left[\frac{v_g x_{e,\text{out}}^2}{\alpha_{\text{out}}} + \frac{v_f (1 - x_{e,\text{out}})^2}{(1 - \alpha_{\text{out}})}\right] - \left[\frac{v_g x_{e,\text{in}}^2}{\alpha_{\text{in}}} + \frac{v_f (1 - x_{e,\text{in}})^2}{(1 - \alpha_{\text{out}})}\right]\right\}$
	$\alpha = \left[1 + \left(\frac{1 - x_e}{x_e}\right)\left(\frac{v_f}{v_g}\right)^{2/3}\right]^{-1}$
	$\Delta P_{\text{sp},g} = \frac{2L_{\text{sp}}}{d_h} f_{\text{sp},g} G^2 v_g$
	$f_{\text{sp},g}\,\text{Re}_g = 24[1 - 1.3553\beta + 1.9467\beta^2 - 1.7012\beta^3 + 0.9564\beta^4 - 0.2537\beta^5]$ $\quad \text{Re}_g < 2{,}000$ $f_{\text{sp},g} = 0.079\,\text{Re}_g^{-0.25}$ $\quad 2{,}000 < \text{Re}_g < 20{,}000$ $f_{\text{sp},g} = 0.046\,\text{Re}_g^{-0.2}$ $\quad 20{,}000 < \text{Re}_g$
	$\text{Re}_{fo} = \frac{Gd_h}{\mu_f}, \text{Re}_f = \frac{G(1 - x_e)d_h}{\mu_f}, \text{Re}_g = \frac{Gx_e d_h}{\mu_g}, \text{We}_{fo} = \frac{v_f G^2 d_h}{\sigma}$
Local boiling Heat transfer coefficient [9]	For $0.05 < x_e \leq 0.55$ $\quad h_{\text{tp}} = 436.48\,\text{Bo}^{0.522}\,\text{We}_{fo}^{0.351}\,X^{0.665} h_{\text{sp},f}$ For $0.55 < x_e$ $\quad h_{\text{tp}} = \max[(108.6X^{1.665} h_{\text{sp},g}), h_{\text{sp},g}]$
	$\text{Bo} = \frac{q''}{Gh_{fg}}, \text{We}_{fo} = \frac{v_f G^2 d_h}{\sigma}$
	$X^2 = \frac{(dp/dz)_f}{(dp/dz)_g}, h_{\text{sp},f} = \frac{\text{Nu}_3 k_f}{d_h}$
	$h_{\text{sp},g} = \frac{\text{Nu}_3 k_g}{d_h}$
	$\text{Nu}_3 = 0.023\,\text{Re}_g^{0.8}\,\text{Pr}_g^{0.4}$ for turbulent gas flow $\text{Nu}_3 = 8.235(1 - 1.883\beta + 3.767\beta^2 - 5.814\beta^3 + 5.361\beta^4 - 2.0\beta^5)$ for laminar gas flow

perature, $T_{w,b}$ (see Fig. 4) along the flow direction for a total evaporator thermal load of $Q_{\text{evap}} = 200$ W and three different values of mass velocity. The local heat transfer coefficient decreases monotonically along the heat sink. Irregularities in this variation are due to the use of discrete correlations for h_{tp} corresponding to different quality regions. The heat transfer coefficient is highest at

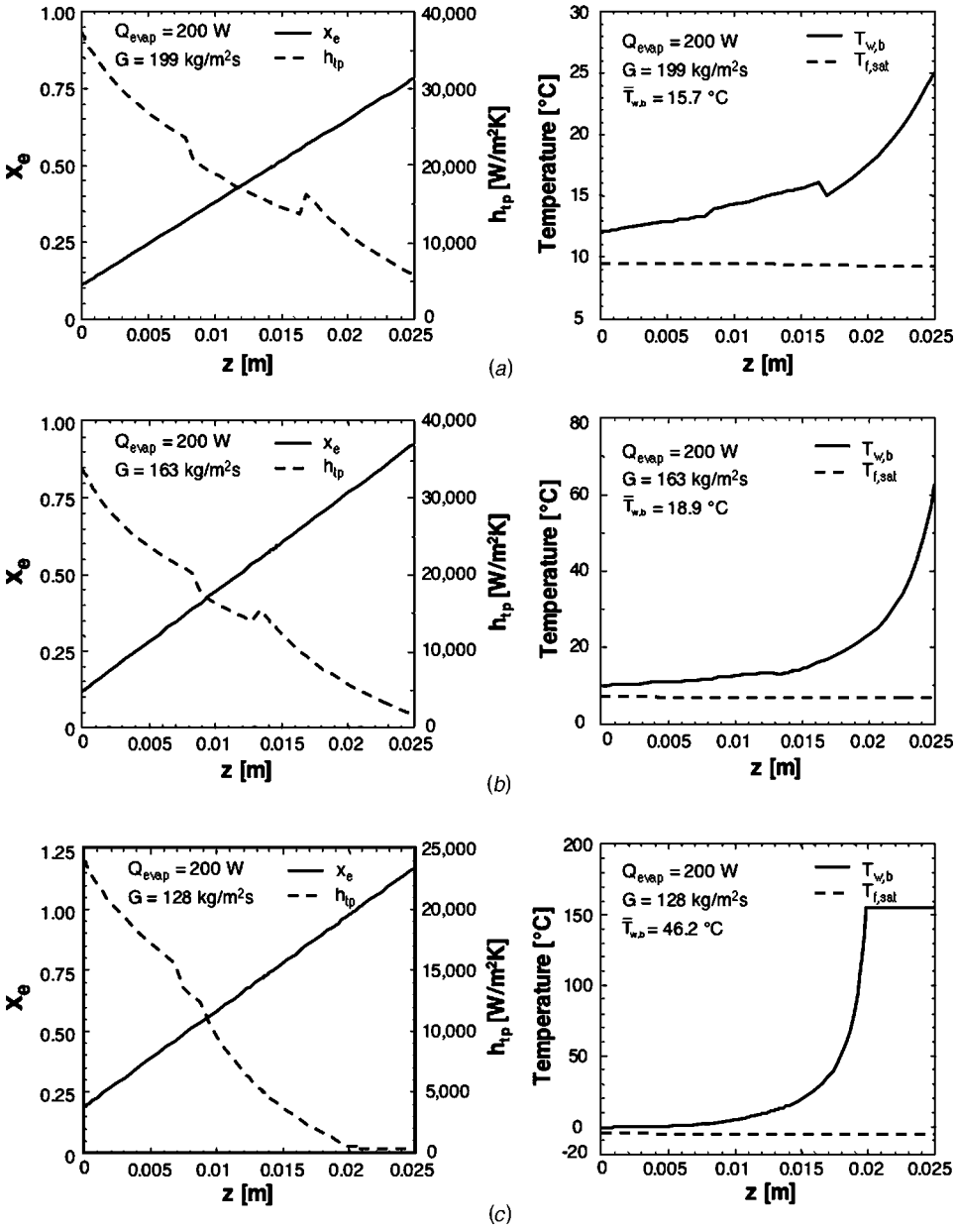

Fig. 8 Predicted variations of quality, two-phase heat transfer coefficient, and channel base temperature along the microchannel for evaporator heat load of 200 W and mass velocities of (*a*) 199, (*b*) 163, and (*c*) 128 kg/m² s

the inlet where liquid is abundant, and decreases sharply in the high quality region, corresponding to localized wall dryout and superheated flow ($x_e > 1$), where the heat is removed mostly by the vapor. Notice the appreciable increase in wall temperature in the high quality region, especially when the evaporator outlet is superheated [Fig. 8(*c*)]. Considering heat sinks are relatively short and made from high conductivity material, the sharp increase in wall temperature depicted in Fig. 8(*c*) for a superheated outlet should be greatly dampened with an actual electronic device. As shown in Fig. 8(*c*), the area–averaged wall temperature, defined as

$$\bar{T}_{w,b} = \frac{\int_0^L T_{w,b} dz}{L}, \tag{2}$$

is much smaller than the outlet temperature. Nonetheless, the localized temperature excursion towards the outlet must be minimized to avoid high thermal stresses. In other words, it is important to pursue acceptable outlet quality values while minimizing the temperature gradient along the heat sink.

5 Parametric Effects of Microchannel Geometry on Heat Sink Performance

To explore the effects of the heat sink's geometrical parameters on cooling effectiveness, several externally determined operating conditions were held constant. First, the heat sink was configured to cool a 2.53×2.53 cm^2 device surface dissipating a uniform heat flux of $q'' = 100$ W/cm^2 (total evaporator heat load of 640 W). Furthermore, refrigerant R134a was assumed to enter the evaporator at $P_{in} = 2.5 \times 10^5$ Pa as a two-phase mixture with a quality of $x_{e,in} = 0.05$. To ensure proper compressor operation (dry compression) and a good COP while precluding appreciable outlet wall temperature rise, the evaporator outlet quality was set at

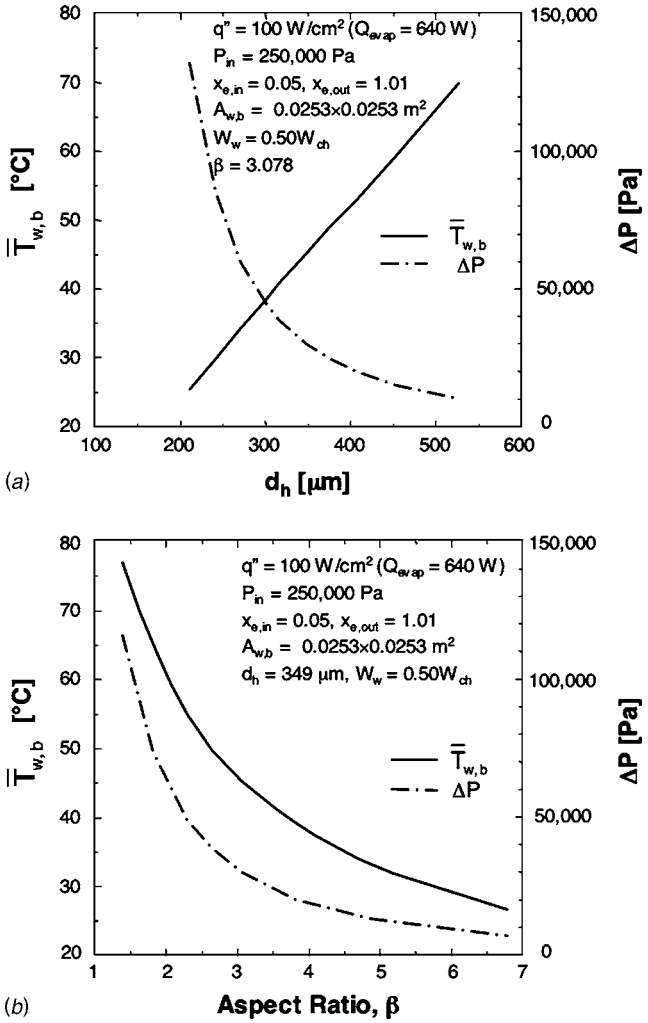

Fig. 9 Variations of mean micro-channel base temperature and pressure drop with (*a*) hydraulic diameter and (*b*) channel aspect ratio

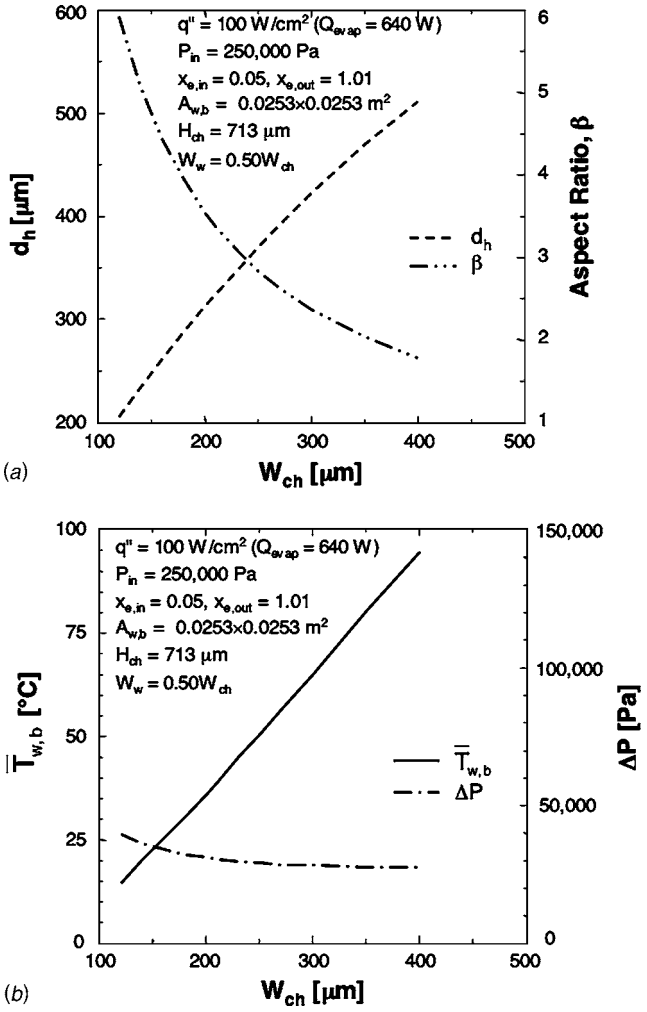

Fig. 10 (*a*) Variations of hydraulic diameter and aspect ratio with channel width for constant channel height. (*b*) Variations of mean channel base temperature and pressure drop with channel width for constant channel height.

$x_{e,\text{out}}=1.01$. Equation (1) was used to determine the mass velocity required to yield this outlet quality value. Finally, the parametric study employed a channel wall thickness equal to the channel width.

Figure 9(*a*) shows the effects of channel hydraulic diameter on heat sink performance for a fixed channel aspect ratio. Lower mean wall temperatures are achieved by decreasing the hydraulic diameter. However, this advantage is realized with a penalty of increased pressure drop. Figure 9(*b*) shows the effects of aspect ratio for a constant hydraulic diameter. Notice, the advantages of reducing both mean wall temperature and pressure drop are realized concurrently by increasing the aspect ratio.

Figure 10 shows the effects of channel width for a fixed channel height. Figure 10(*a*) shows reducing the channel width for a fixed height decreases the hydraulic diameter while increasing the aspect ratio. Figure 10(*b*) shows decreasing channel width produces the desired decrease in mean wall temperature, brought about mainly by reducing the hydraulic diameter. By maintaining a high aspect ratio, the same decrease in channel width is shown yielding only a modest increase in pressure drop. These findings point to a very important tactic in designing microchannel evaporators: using narrow microchannels with a high aspect ratio.

6 Conclusions

This study was performed to explore optimum conditions for incorporating a microchannel heat sink as an evaporator in a refrigeration loop. Experimental measurements and numerical results were used to assess the thermal performance of the heat sink in relation to the performance of the refrigeration cycle. Key conclusions from the study are as follows:

(1) Utilizing a microchannel heat sink as an evaporator in refrigeration loop provides several important thermal benefits such as high-flux dissipation, low surface-to-coolant resistance, and most importantly low device temperature.
(2) Higher heat transfer coefficients are possible with greater mass velocities. However, greater mass velocities are typically associated with wet compression conditions corresponding to evaporator exit quality below unity and liquid entrainment at the compressor inlet. Wet compression compromises compressor performance and reliability as well as refrigeration cycle efficiency. Wet compression must therefore be minimized by maintaining only slightly superheated conditions at the compressor inlet, or using a wet-compression-tolerant compressor.
(3) Another thermal disadvantage of a superheated evaporator outlet is the likelihood of a localized increase in the solid wall temperature towards the outlet, which can cause large thermal stresses at the same location. Practical solutions are therefore needed to develop systems which are both wet compression tolerant and that include adaptive flow control to maintain the desired evaporator outlet quality.

(4) A parametric study of the effects of channel geometry on heat sink performance points to channels with small width and high aspect ratio as yielding superior thermal performance corresponding to only a modest penalty in pressure drop.

Acknowledgment

The authors are grateful for the support of the Office of Naval Research (ONR) for this research.

Nomenclature

$A_{w,b}$ = total base area of heat sink
Bo = boiling number
C = two-phase multiplier parameter
C_c = contraction coefficient
COP = coefficient of performance, ratio of heat sink (evaporator) thermal load to compressor power consumption
d_h = hydraulic diameter
f = fanning factor
G = mass velocity ($kg/m^2\,s$)
h = heat transfer coefficient ($W/m^2\,K$); enthalpy (J/kg)
H_{ch} = microchannel height
H_{tc} = distance between thermocouple and base of the microchannel
k = thermal conductivity (W/m K)
L = length
L_{tc} = axial location of thermocouple
Nu = nusselt number
P = pressure (Pa)
ΔP = pressure drop
Pr = Prandtl number
q'' = heat flux through heat sink base area (W/m^2 or W/cm^2)
Q_{evap} = total evaporator (heat sink) heat load (W)
Re = Reynolds number based on channel hydraulic diameter
T = temperature
T_{tc} = measured copper temperature
$T_{w,b}$ = base temperature of microchannel
$\bar{T}_{w,b}$ = mean base temperature of microchannel
v = specific volume (m^3/kg)
W_{ch} = microchannel width
W_w = half-width of wall separating microchannels
We = Weber number
X = Martinelli parameter
x_e = thermodynamic equilibrium quality
z = streamwise coordinate

Greek

α = void fraction
β = channel aspect ratio (height/width)
μ = viscosity
σ = surface tension
σ_c = contraction area ratio
σ_e = expansion area ratio
ϕ = two-phase multiplier

Subscripts

3 = three-sided wall heating
a = acceleration
c = contraction
ch = microchannel
e = thermodynamic equilibrium; expansion
f = saturated liquid; frictional
fg = property difference between saturated liquid and saturated vapor
fo = liquid only in entire channel
g = saturated vapor
in = channel/evaporator inlet
out = channel/evaporator outlet
sat = saturated
sp = single-phase
tp = two-phase
tot = total
vv = laminar liquid and laminar vapor
vt = laminar liquid and turbulent vapor

References

[1] Tuckerman, D. B., and Pease, R. F. W., 1981, "High-performance Heat Sinking for VLSI," IEEE Electron Device Lett., **2**, pp. 126–129.
[2] Bowers, M. B., and Mudawar, I., 1994, "High Flux Boiling in Low Flow Rate, Low Pressure Drop Mini-Channel and Micro-Channel Heat Sinks," Int. J. Heat Mass Transfer, **37**, pp. 321–332.
[3] Qu, W., and Mudawar, I., 2003, "Measurement and Prediction of Pressure Drop in Two-Phase Micro-Channel Heat Sinks," Int. J. Heat Mass Transfer, **46**, pp. 2737–2753.
[4] Qu, W., and Mudawar, I., 2003, "Flow Boiling Heat Transfer in Two-Phase Micro-Channel Heat Sinks—I. Experimental Investigation and Assessment of Correlation Methods," Int. J. Heat Mass Transfer, **46**, pp. 2755–2771.
[5] Mikic, B. B., Rohsenow, W. M., and Griffith, P., 1970, "On Bubble Growth Rates," Int. J. Heat Mass Transfer, **13**, pp. 657–665.
[6] Mudawar, I., 2001, "Assessment of High-Heat-Flux Thermal Management Schemes," IEEE Trans. Compon. Packag. Technol., **24**, pp. 122–141.
[7] Schmidt, R., 2000, "Low Temperature CMOS Experience at IBM," 16th IEEE SEMI-Therm Symp., San Jose, CA, March 21–23, pp. 112–113.
[8] Lee, J., and Mudawar, I., 2005, "Two-Phase Flow in High-Heat-Flux Micro-Channel Heat Sink for Refrigeration Cooling Applications: Part I—Pressure Drop Characteristics," Int. J. Heat Mass Transfer, **48**, pp. 928–940.
[9] Lee, J., and Mudawar, I., 2005, "Two-Phase Flow in High-Heat-Flux Micro-Channel Heat Sink for Refrigeration Cooling Applications: Part II—Heat Transfer Characteristics," Int. J. Heat Mass Transfer, **48**, pp. 941–955.